Journal of Applied Polymer Science

Enhanced dielectric properties of polyamide 11/multi-walled carbon nanotubes composites

Yongzhong Huang,[1] Lirong Tan,[1] Shaodi Zheng,[1] Zhengying Liu,[1] Jianming Feng,[1] Ming-Bo Yang[1,2]
[1]College of Polymer Science and Engineering, Sichuan University, Chengdu 610065, People's Republic of China
[2]State Key Laboratory of Polymer Materials Engineering, Sichuan University, Chengdu 610065, People's Republic of China
Correspondence to: Z. Liu (E-mail: liuzhying@scu.edu.cn)

ABSTRACT: Composites with multi-walled carbon nanotubes (MWNTs) involved in polyamide 11 (PA11) were prepared via a conventional melt blending method. The structure, morphology, crystallization behavior, electrical, and dielectric properties of composites were investigated. The results demonstrated that the dispersed uniformly MWNTs favored the formation of α crystal of PA11 when the composites were quenched from melt. The dielectric constant of composites was dependent on the electric field frequency and MWNTs content, and the highest value of dielectric constant was as high as 350 for the composite with 1.21 vol % MWNTs at 10^3 Hz, accompanied by a low dielectric loss. The enhanced dielectric properties could be interpreted by the formation of abundant nanocapacitors within the composites and the interfacial polarization effect resulting from accumulation of charge carriers at the internal interfaces between MWNTs and PA11. © 2015 Wiley Periodicals, Inc. J. Appl. Polym. Sci. **2015**, *132*, 42642.

KEYWORDS: composites; dielectric properties; nanostructured polymers; polyamides

Received 12 April 2015; accepted 21 June 2015
DOI: 10.1002/app.42642

INTRODUCTION

With the rapid development of information, electronic and electric power industry in recent years, polymer-based dielectric materials with high dielectric constant and low dielectric loss have attracted intensive interest on account of their potential applications such as electric energy storage devices, flexible electronics, artificial muscles, and sensors.[1–4] Traditionally, one common approach to improve the dielectric constant of polymer is to disperse insulating ceramic powder with high dielectric constant such as $PbTiO_3$ and $BaTiO_3$ into polymer matrix. However, the applications of such composites are seriously limited, because a large amount of ceramics are usually required for the purposed industrial applications, thus resulting in the deterioration of mechanical and processing properties like flexibility and compatibility. Another universal method to prepare dielectric materials is introducing electric conductive fillers into polymer matrix, among which, the CNTs have been always chosen as fillers to enhance the electrical, thermal, and mechanical properties of the composites because of their high aspect ratio and large specific surface area.[5–9] Furthermore, compared with ceramic/polymer composites, a small loading of CNTs is sufficient to obtain a high dielectric constant.[10] Zhang *et al.*[11] prepared a CNT/P (VDF-TrFE-CFE) nanocomposite via a coagulation method. The dielectric constant enhancement is 30% for the nanocomposite with merely 1.0 wt % CNTs compared with the pure P (VDF-TrFE-CFE). Li *et al.*[12] fabricated carboxylic and ester functionalized multi-walled carbon nanotube (MWNTs) /PVDF composites by evaporating suspensions of the nanotubes in PVDF. They demonstrated that chemical functionalized MWNTs could improve the dielectric properties of composites significantly. The highest dielectric constant of 3600 was obtained in the carboxylic functionalized MWNTs/PVDF composite with only 8 vol % MWNTs at 1 kHz.

The dielectric constant of the conductive particle-polymer composites (CPCs) can be several orders of magnitude higher than that of the insulating polymer matrix, but it is not a direct consequence of intrinsic dielectric permittivity value of fillers and host polymer as in the case of ceramic-polymer composites. A number of models considering different mixing rules have been proposed and used for predicting the effects of second phases on the dielectric properties of the composite, such as Maxwell-Garnett equation,[13,14] Jaysundere-Smith equation,[15] Lichtenker rule,[16] and percolation model.[17] Previous studies[17–19] have reported that the dielectric properties of the CPCs can be tailored by the type and level of reinforcement, size and shape of filler, type of matrix, and the composites preparation methods. All the factors are inter-related and should be considered systemically when developing a new material with high dielectric constant. Besides the preparation methods, solution-mixing method can ensure the great dispersion of fillers in the polymer

matrix, and enhance the dielectric properties of composites. Yang *et al.*[20] prepared carbon nanofiber (CNF)-polystyrene (PS) composites by ultrasonic dispersion in a solution followed by spraying to cast films, and the results showed that the dielectric constant of CNF-PS composites can reach more than 80 at a frequency of 15 GHz. He *et al.*[21] adopted a solution precipitation method to obtain graphite/PVDF composites. When the graphite loading amount was 10 wt %, the dielectric constant at 10^4 Hz were approximately 83% and 93% higher than those of pure PVDF, respectively. In addition, melt-blending is another universal and effective method to prepare polymer-based composites with excellent dielectric properties. Jin-Kai Yuan *et al.*[22] prepared pristine MWNTs/PVDF composite through the melt-blending procedure, and found that the resultant nanocomposite possesses a giant dielectric constant (3800) of three orders of magnitude higher than the PVDF matrix, which was attributed to the reinforced interfacial effect based on the remarkable molecular level interaction. Furthermore, the high dielectric constant is not sufficient for the application of dielectric materials, low dielectric loss is also important. Ning *et al.*[23] obtained MWNTs/ PVA composites with high dielectric constant and low dielectric loss by controlling the alignment of MWNTs via electrospinning—*in situ* film—forming technique, and ascribed the improved dielectric properties to good dispersion and alignment of MWNTs in the matrix resulting in a large number of separated nanocapacitors. Recently, an innovative approach was utilized to increase the dielectric constant and reduce the dielectric loss of MWNTs/polymer composites by using a particular core-shell structured MWNTs as fillers.[24,25] The outer walls of MWNTs were covalently functionalized to become non-conductive, while the inner walls were remained electrically conductive. Besides, MWNTs/polymer composites with high dielectric constant and low dielectric loss can also be achieved by introducing insulating modification layers on the surface of MWNTs. Yang *et al.*[25] successfully prepared flexible dielectric MWNTs/polystyrene composites by coating an organic polypyrrole (PPy) shell on the MWNTs surface, and found the resultant composite possesses a high dielectric constant ($\approx$44) and a rather low dielectric loss ($<$0.07). The coating of PPy shell on the MWNTs surfaces can ensure the good dispersion of MWNTs in the matrix and prevent MWNTs from connecting with each other to shut off the leakage current which contributes to the dielectric loss.

Polyamide-11 (PA11) is an important commercial polyamide with excellent ferroelectric properties and has been widely used in a large range of industrial fields such as automotive and offshore applications.[26–28] Former studies of PA11 showed that it has five different crystal phases: the triclinic α phase, the monoclinic β phase and three hexagonal or pseudo-hexagonal phases (γ, γ' and δ').[29,30] The polymorphs of PA11 are dependent on crystallization condition and thermal history. Up to now, semicrystalline polymer PVDF has always been chosen as matrix to prepare dielectric composites because of its relatively high dielectric constant at room temperature and superior ferroelectric performances.[31–33] Furthermore, the dielectric properties of polymer have a close relationship with intrinsic polarity. Just as PVDF, PA11 is also a polar polymer matrix and few studies have been focused on the dielectric properties of PA11/MWNTs composites yet. In this study, PA11/MWNTs composites are prepared by blending pristine MWNTs with PA11 in molten state using a small torque rheometer. The melt mixing is a promising route to achieve homogenous dispersion of CNTs in the polymer matrix because of the chemical and/or physical interaction between CNTs and macromolecules of polymer caused by the high temperature and shear forces. Then the dielectric and electric properties as well as the crystal structure and crystalline behavior of the composites were investigated.

EXPERIMENTAL

Materials and Sample Preparation

Semicrystalline polymer PA11 pellets (BESN–P40TL, Arkema Group, France) were used as polymer matrix. The MWNTs (NC 7000) were obtained from Nanocyl S.A. (Belgium). According to the manufacturer, the MWNTs were produced by the chemical vapor deposition method and had an average diameter of 10 nm, length of 1.5 μm and specific surface area of 250–300 $m^2\ g^{-1}$.

A range of PA11/MWNTs composites containing 0, 0.12, 0.3, 0.602, 0.905, 1.21, 2.44 vol % were prepared via melt blending using a HAAKE torque rheometer (XSS-300) at 210°C with a screw speed of 70 rpm. All PA11 pellets were dried in vacuum oven at 80°C for 24 h before melting process. Then composites samples were prepared by compression molding at 210°C and pressure of 10 MPa for 5 min, and quenched into ice water afterwards. For the alternating current (ac) conductivity and dielectric properties measurement, the samples were pressed into disk-shape with 10 mm in diameter and 1.5 mm in thickness at 10 MPa, and then quenched into ice water.

Characterization of Composites

Scanning Electron Microscopy Analysis. The morphology of composites was examined by scanning electron microscopy (SEM) using an Inspect F instrument at an accelerating voltage of 20 kV. The sample surfaces for SEM examination were prepared by cryogenic fracture in liquid nitrogen and coated with a thin layer of gold.

Differential Scanning Calorimetry Analysis. Thermal characterization of PA11/MWNTs composites were performed with a Differential scanning calorimetry (DSC, Q20, TA Instruments, USA) instrument calibrated with indium under a nitrogen atmosphere. The samples were heated from 30°C to 210°C at a rate of 10°C /min to record the melting behavior of samples.

Wide-Angle X-ray Diffraction Analysis. Wide-angle X-ray diffraction (WAXRD) patterns of the as-prepared samples were performed using DX-1000 X-ray diffractometer (Dandong Fanyuan Instrument) with CuK_α radiation ($\lambda = 1.54$ Å), operated at 40 mA current and 40 kV voltages. The diffraction traces were obtained over a two theta (2θ) range of 5° to 45°.

FTIR Analysis. Room temperature infrared spectra of the samples were performed on a Nicolet 6700 FTIR spectrometer (Thermo Electron) in the reflection mode. The wavelength range is 500–3600 cm^{-1} and the resolution is 4 cm^{-1}.

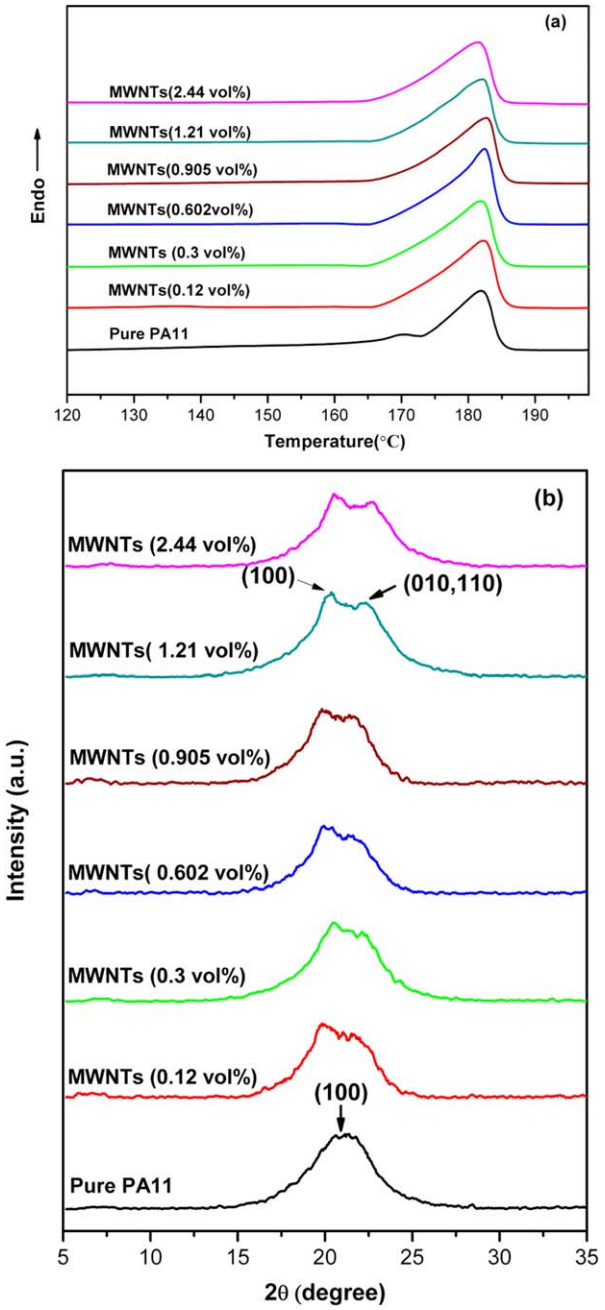

Figure 1. (a) DSC curves and (b) WAXRD pattern of pure PA11 and PA11/MWNTs composites. [Color figure can be viewed in the online issue, which is available at wileyonlinelibrary.com.]

Electrical Characterization. The direct current (DC) electrical properties of the composites were measured by a Keithley 6517B electrometer (Keithley Instruments, Ohio). Prior to the measurements, electrodes of silver were painted on the opposite sides of samples. The alternating current (AC) electrical properties of the composites were performed using Agilent 4294A precision LCR meter in the frequency range of 10^3-10^7 Hz at room temperature.

Dielectric Characterization. The AC frequency dependent values of parallel capacitance (C_p) and dissipation factor (tanδ) of the nanocomposite samples were also contained using Agilent 4294A precision LCR meter. Dielectric constant (ε) was calculated using the formula:

$$\varepsilon = C/C_0 \quad (1)$$

where C_0 ($=\xi_0 A/d$) is the capacitance with vacuum between parallel plates, and ξ_0 is the vacuum permittivity (8.854×10^{-12} F/m), A is the area of electrodes, and d is the thickness of the sample. Dissipation factor (tanδ) was directly obtained on the LCR meter.

RESULTS AND DISCUSSION

Crystal Structure and Crystallization Behavior of Composites

The DSC thermogram of pure PA11 and PA11/MWNTs composites is shown in Figure 1(a). The T_m (melting temperature) and ΔH_m (melting heat of crystallization) are obtained from the DSC results and listed in Table I. The degree of crystallinity of a specimen can be calculated from the melting heat of crystallization according to the following equation:

$$X_{c,h} = \Delta H_m / \Delta H_0 \quad (2)$$

where ΔH_0 =189.05 J/g is the enthalpy of fusion for the perfectly crystalline PA11.[34] The T_m and calculated degree of crystallinity ($X_{c,h}$) of composites are slightly higher than that of pure PA11, but almost independent on the MWNTs content. Previous studies have revealed the nucleation effect of carbon nanotubes in poly (ε-caprolactone) (PCL), poly (ethylene terephthalate) (PET), polyamide 6 (PA6), and PA66.[35–38] Yang *et al.*[39] demonstrated that MWNTs played two competing effects on the crystallization of PA11 composites: acting as nucleation medium to promote crystallization, and physic hindrance to retard crystal growth of matrix. The low content of MWNTs could facilitate the mobility of the PA11 molecular chains and brought heterogeneous nucleation effects simultaneously, thus increasing the degree of crystallinity. As the content of MWNTs increased, they obstructed the mobilization of the PA11 molecular chains and prevented molecular segments from obtaining ordered alignment of the crystal lattice, resulting in lower degree of crystallinity. But in our study, when the samples were cooled very quickly from the melt, the crystalline process of PA11 was controlled dominantly by the fast cooling rate, so the effects of MWNTs on the crystalline behavior were concealed, and the overall degree of crystallinity was almost invariable despite the increasing MWNTs content.

Figure 1(b) presents the WAXRD patterns of the pure PA11 and PA11/MWNTs composites. It can be seen that the pure PA11 exhibits only one strong and broad (100) reflection at the diffraction angle 2θ of 21.3°, which is characteristic of the pseudo-hexagonal δ' crystal phase of PA11 produced by quenching specimens into ice water.[40] The piezoelectricity and ferroelectricity of PA11 is derived from this δ' phase. As MWNTs are added into the matrix, the (100) reflection of the δ' phase splits into two reflections. For the composites with low content of MWNTs, the two reflections are not very apparent. However, the two reflections are strong and distinct for the composites with 1.21 vol % MWNTs, and the corresponding diffraction angel 2θ are 20.04° and 23.12°, which can be indexed as (100) and (010,110) lattice plane of α crystal phase.[41] It can be

Table I. Crystallization Parameters of Pure PA11 and PA11/MWNTs Composites

	T_m (°C)	ΔH_C (J/g)	$X_{c,h}$ (%)	$X_{c,x}$ (%)
Pure PA11	181.98	37.35	19.76	21.96
PA11/MWNTs (0.12 vol %)	182.30	39.86	21.13	23.74
PA11/MWNTs (0.3 vol %)	181.90	40.69	21.64	24.31
PA11/MWNTs (0.602 vol %)	182.43	41.47	22.16	24.62
PA11/MWNTs (0.905 vol %)	182.73	41.01	22.02	24.87
PA11/MWNTs (1.21 vol %)	182.15	39.86	21.08	24.82
PA11/MWNTs (2.44 vol %)	181.44	40.71	21.53	23.95

concluded that the addition of MWNT has an influence on the crystal phase of PA11.

The degree of crystallinity ($X_{c,x}$) calculated with WAXRD data are also listed in Table I, according to the following equation:

$$X_{c,x}=\frac{I_{100}+1.57I_{010,110}}{I_{100}+1.57I_{010,110}+0.811I_a} \quad (3)$$

In this equation, I refers to integrated intensity of diffraction peak; I_a is the integrated intensity of amorphous peak in 20.8°. The calculated degree of crystallinity is also almost independent of the MWNTs content, but slightly higher than that of calculated from DSC results. This difference lies in the fact that WAXRD calculation is based on the electron density difference between crystalline and amorphous area, while DSC calculation is based on the crystallization enthalpy. Discussing DSC and WAXRD results together, conclusions can be gained that the MWNTs contents do not influence the degree of crystallinity when the samples are cooled very quickly from melt, but favor the formation of stable α crystal phase of PA11, while pure PA11 represents the metastable δ' phase. In our experiments, on account of the quenching condition, although the nucleation center of PA11 was formed, it did not have enough time to grow stable crystal because of the large cooling rate. So the metastable δ' phase was formed, and this metastable phase was a production of dynamics. However, for the PA11/MWCNTs composites, it was feasible to form stable crystal under such short crystallization duration owing to the heterogeneous nucleation effect of MWNTs. Meanwhile, the crystallization degree were relatively low under this quenching condition, and only the local polymer chains surrounding the nucleation centers would participate in the crystal growth process. Hence the MWNTs had little possibility to obstruct whole polymer chains' mobility, and all the composites showed almost similar crystallization behavior without regard to the filler contents. As a result, the PA11/MWNTs composites developed the stable α phase, while pure PA11 represented the metastable δ' phase. These results can be further confirmed by FTIR in the following paragraph.

FTIR spectra of nylons with four important regions has been well documented in the literature.[42] The region at 500–800 cm^{-1} contains the amide V and VI bands. The 1000–1400 cm^{-1} region contains the so-called progression bands and is sensitive to methylene segments. The region 1500–1800 cm^{-1} comprises the amide I and II bands which are both sensitive to the N—H stretching and C—O bonds. The amide A band at about 3300 cm^{-1} is assigned to N—H stretching vibration that is sensitive to the strength of the hydrogen bond. The contribution to the amide A comes from free N—H stretching at 3444 cm^{-1}, bonded N—H stretching at 3300 cm^{-1} arising out of crystalline fraction, and bonded N—H stretching at 3310 cm^{-1} arising out of amorphous fraction. The room-temperature spectra of the four regions of pure PA11 and PA11/MWNTs composites are shown in Figure 2(a–d). Obviously, the peak wave numbers of composites are distinctly different from the pure PA11, but show very subtle differences between the composites with different MWNTs contents. Figure 2(a) shows that the amide V and VI bands appear at 694 and 588 cm^{-1} respectively for the pure PA11, but occur at about 686 and 582 cm^{-1} for the PA11/MWNTs composites. Figure 2(b) compares the progression bands at 1000–1400 cm^{-1} region of pure PA11 and PA11/MWNTs composites .The bands appear at 1113, 1148, 1209, 1263 cm^{-1} for the pure PA11, however, appear at 1121, 1157, 1221, 1276 cm^{-1} for the composites respectively. The amide I and II bands appear at 1644 and 1548 cm^{-1} for the pure PA11, but appear at about 1538 and 1636 cm^{-1} for the composites, respectively [Figure 2(c)]. From Figure 2(d), the amide A band appears at 3295 cm^{-1} for the pure PA11, in the case of composites, it shifts from 3306 to 3310 cm^{-1} with increasing MWNTs contents. To sum up, the composites show distinct difference compared with the pure PA11 in the four regions of the FTIR spectra. Since the conformation in the amorphous is expected to be the same for all the phases, the difference may be attributed to the different conformation of δ' and α phases. Moreover, the MWNTs surface has zigzag carbon atoms which match well with the all-trans conformation of α phase of PA11, so the difference also origins from the influence of MWNTs in the PA11 matrix.

Dispersion of MWNTs in the PA11 Matrix

It is widely accepted that the dispersion state of MWNTs involved in polymer matrix can be totally different depending on the magnification or scales. So it is important to clearly define the dispersion based on the different scales. Here, Figure 3(a–d) shows the SEM micro-morphology of the cryo-fractured surface of composite with the 2.44 vol % MWNTs under different magnification levels. The bright dots in the PA11 matrix are attributed to the ends of broken MWNTs because of their high conductivity. It is clearly found that MWNTs are uniformly dispersed in the matrix, and little agglomerates are observed (part c and d of Figure 3), and no MWNTs are pulled out in the

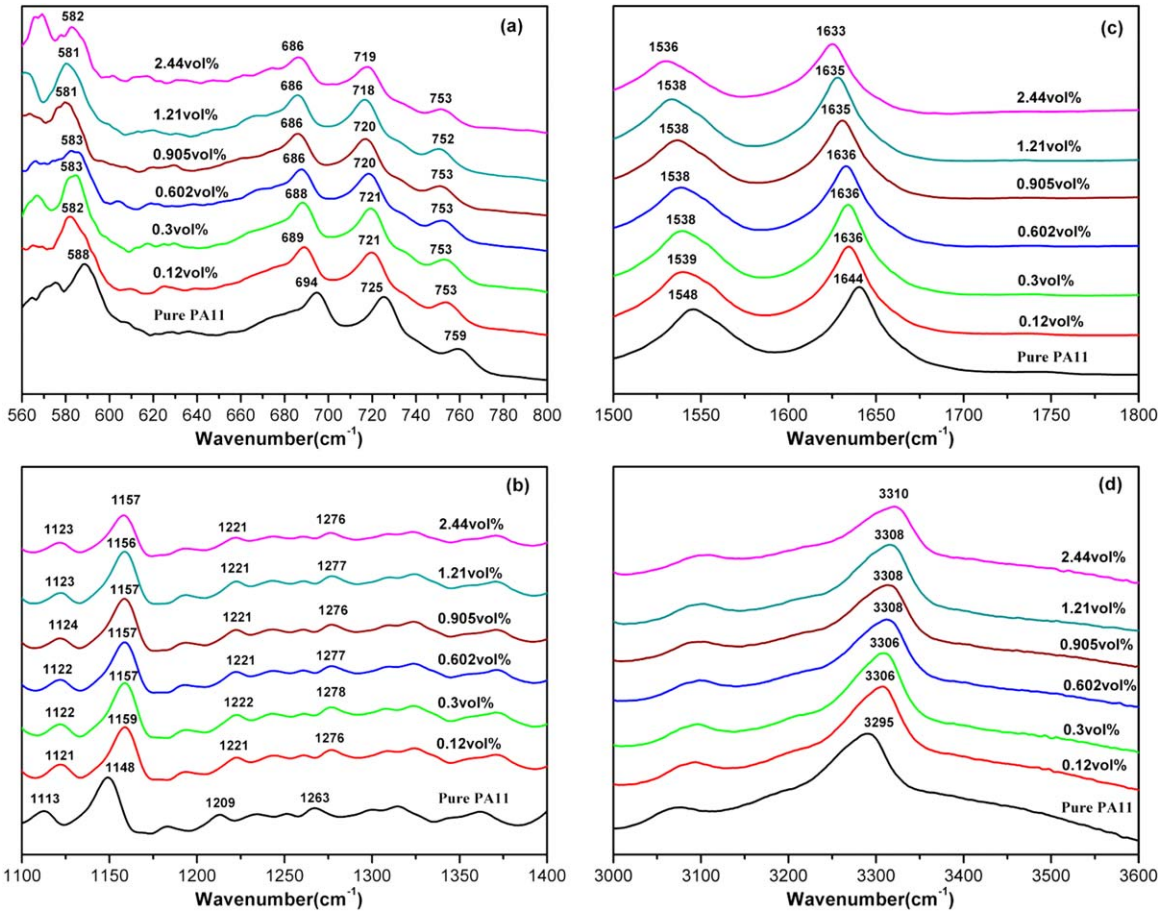

Figure 2. Room-temperature FTIR spectra of pure PA11 and PA11/MWNTs composites of the region: (a) 500–800 cm^{-1}, (b) 1100–1400 cm^{-1}, (c) 1500–1700 cm^{-1}, and (d) 3300–3600 cm^{-1}. [Color figure can be viewed in the online issue, which is available at wileyonlinelibrary.com.]

breaking process and no interfacial debonding was seen. Moreover, uniform distribution of individual MWNTs throughout the composites can be confirmed by SEM at lower magnification level [Figure3(a,b)].

Electric Properties of the Composites

Figure 4 displays the evolution of the DC conductivity of PA11-based composites as a function of MWNTs content. It is observed that a stair-step increase in electrical conductivity occurs with increasing MWNTs content. A minor increase in DC conductivity from 4.4×10^{-10} to 9.3×10^{-9} S/m is observed when only 0.12 vol % of MWNTs is added into pure PA11 matrix. After that, when the MWNTs content are 1.21 vol % and 2.44 vol %, the DC conductivity value reach to 8.1×10^{-6} and 9.6×10^{-4} S/m respectively, both of which are conducting materials. The conductivity can be further analyzed with the critical MWNTs content f_c by the following scaling law near the conductor–insulator transition as follows:[43,44]

$$\sigma \propto \sigma_i (f_c - f_{\mathrm{MWNTs}})^{-s} \quad \text{for} \quad f_{\mathrm{MWNTs}} \ll f_c, \tag{4}$$

where σ is the conductivity of the composites, σ_i is the conductivity of the insulating PA11 polymer, f_{MWNTs} is the MWNTs volume fraction, f_c is the percolation threshold, s is the critical exponent in the insulating region. The best fits of the conductivity data to the log–log plots of eq. (4) scaling law gives $f_c \approx$ 1.04 vol %, and $s = 2.4$, as shown the insets in Figure 4. The exponent s is larger than the universal one ($s = 0.8$–1),[43,44] and this discordance probably derives from the fact that the electrical connectivity in composites is achieved by tunneling because of the formation of a much thin PA11 layer around the MWNTs walls, which prevents the direct physical contact between the nanotubes.

Figure 5(a) shows the AC electrical conductivity of the pure PA11 and PA11/MWNTs composites with various MWNTs content as a function of electric field frequency at room temperature. AC conductivity [σ_{AC} (ω)] is frequency-dependent and follows a universal power expressed as

$$\sigma_{AC}(\omega) = \sigma_{DC} + A(\omega)^S \quad (0 < S < 1) \tag{5}$$

where σ_{DC} is the DC conductivity, ω is the angular frequency, A and S are parameters dependent on both frequency and temperature. As depicted in Figure 5(a), AC conductivity of the pure PA11 and composites with different MWNTs content show different dependence on the applied electric field frequency. For pure PA11 and composites with 0.12 vol % MWNTs, electrical conductivity is almost linearly dependent on the frequency. But for the composites with 0.3 vol % MWNTs, a frequency independent plateau up to a critical frequency (ω_c) is observed, which indicates the direct current conductivity and

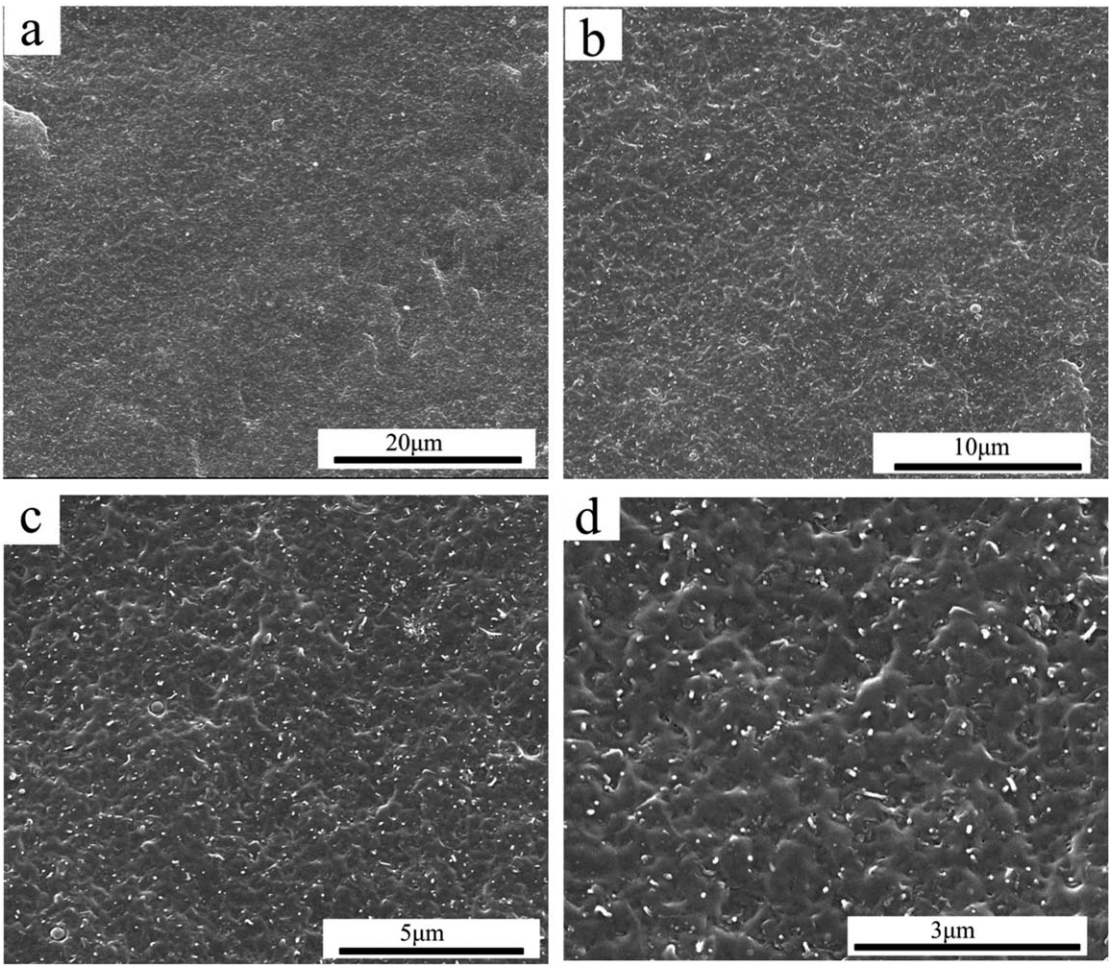

Figure 3. SEM images of the fractured surface of composites with 2.44 vol % MWNTs under different magnifications: (a) 5 k, (b) 10 k, (c) 20 k, (d) 40 k.

nondielectric behavior of composites at low frequency occurs. It is further noticed that the value of critical frequency (ω_c) extends to higher frequencies with increasing volume fraction of MWNTs. An obvious increase in conductivity is observed for the PA11/MWNTs composites with 2.44 vol % MWNTs where the electrical conductivity is almost invariable over a wide range of frequency, indicating the conquering role of Ohmic conduction and stability of well-established conductive network formation in composites. Figure 5(b) displays the AC conductivity of the pure PA11 and PA11/MWNTs composites as a function of MWNTs content measured at room temperature. It can be seen that for the pure PA11 and composites with 0.12 vol % MWNTs, electrical conductivity are $\sim 10^{-10}$ and 10^{-9} S/m at 10^3 Hz, respectively. This low electrical conductivity demonstrates that pure PA11 and composites with low MWNTs content are electrically insulating materials. Then the conductivity of composites increases gradually with increment of MWNTs content at a constant frequency, and reaches a relatively high value for the composites with 2.44 vol % MWNTs which indeed are electrical conductive materials. It can be comprehended by conventional electric conduction theory: the formation of conduction network with the increase of conductive fillers content.

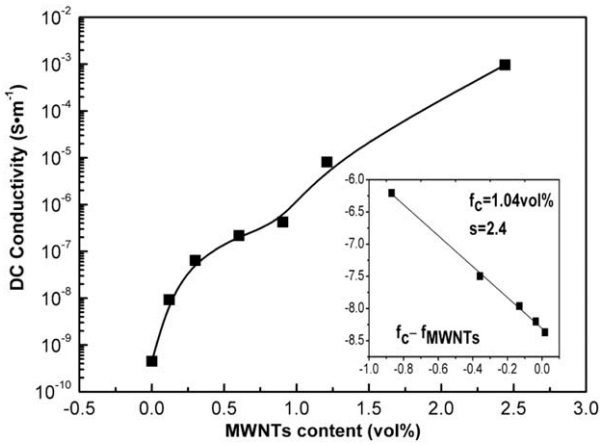

Figure 4. DC conductivity of pure PA11 and PA11/MWNTs composites as a function of MWNTs content; the inset shows a log–log plot of the conductivity as a function of f_c–f_{MWNTs} according to eq. (4).

Dielectric Properties of the Composites

The ability of dielectric materials to store energy is attributed to polarization, i.e. electric field-induced separation and alignment of electric charges, which will result in an increase in

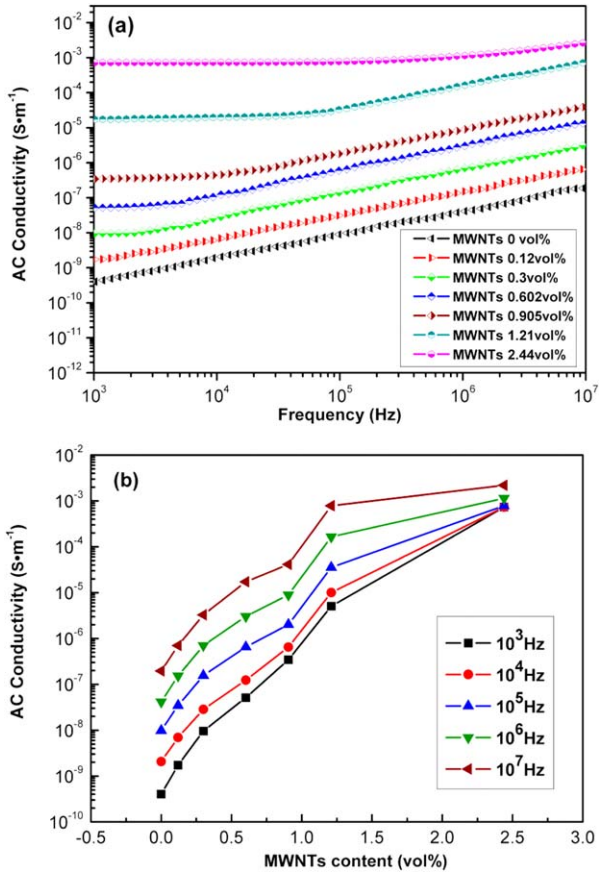

Figure 5. (a) AC electrical conductivity of pure PA11 and PA11/MWNTs composites with various MWNTs contents as a function of frequency; (b) electrical conductivity of pure PA11 and PA11/MWNTs composites at the variation of the frequency from 10^3 to 10^7 Hz. [Color figure can be viewed in the online issue, which is available at wileyonlinelibrary.com.]

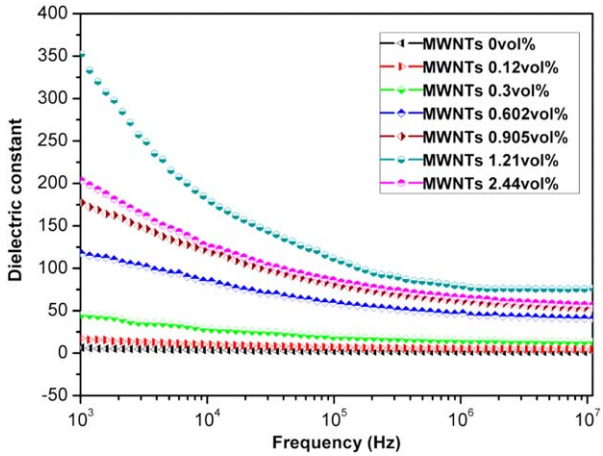

Figure 6. Frequency dependence of the dielectric constant of pure PA11 and PA11/MWNTs composites with different MWNTs contents. [Color figure can be viewed in the online issue, which is available at wileyonlinelibrary.com.]

capacitance. Figure 6 shows the variation of dielectric constant of pure PA11 and its composites with MWNTs as a function of frequency at room temperature. The dielectric constant demonstrates a slight correlation to the frequency when the MWNTs content is smaller than 0.12 vol %, and the pure PA11 even keeps almost unaltered dielectric constant over the whole range of frequency. However, when the MWNTs content is higher than 0.3 vol % especially for the composites with 1.21 vol % MWNTs, the dielectric constant decreases dramatically with increasing frequency. As we know, the polarizability can usually be separated into electronic contribution, ionic contribution, and dipole contribution. At low frequency, all of these parts contribute to the dielectric constant. When the frequency increases, the space charges and permanent dipoles are difficult to keep in pace with the rapidly changing electrical vector, and they "relax out" at some frequency. Therefore, the overall polarization effect decreases, and the value of dielectric constant also decreases consequently as it is directly proportional to the degree of polarization. So it is the reason for the strong dependence of dielectric constant on frequency for the composites with above 0.3 vol % MWNTs. Furthermore, the existence of dipole oscillation in an electric field depends upon the nature of the local environment. As described in the previous paragraph, the addition of MWNTs favors α crystal phase of PA11, but the pure PA11 quenched in ice water represents the δ' phase. The intersheet distance between the hydrogen-bonded sheets of δ' phase is larger than that of α crystal phase, and its hydrogen bonding direction is randomly pointed along the chain backbone and the adjacent chains. So the movement freedom of the polar groups is greater in the δ' phase than α phase.[45,46] Moreover, the diffusion of localized charge carriers and movement of polar groups is easier (less barrier) for the pure PA11 because of the absence of MWNTs which would absorb the molecular chains on its surface and hinder the mobilization of the molecular segments and chains. Therefore, the dielectric constant are strongly dependent on frequency for the composites with high MWNTs contents, but shows tiny frequency dependence for the pure PA11 and composites with 0.12 vol % MWNTs.

The dielectric constants measured at 10^3, 10^4, 10^5, 10^6, and 10^7 Hz of pure PA11 and PA11/MWNTs composites are compared and shown in Figure 7(a). As generally expected, the dielectric constant of composites would be significantly enhanced compared with that of the pure PA11 (about 7 at 10^3 Hz). It is found that the dielectric constant reaches a maximum value to 350 at10^3 Hz for the composites with 1.21 vol % MWNTs, almost 50 times that of the pure PA11. The large enhancement of the dielectric constant at low frequency is attributed to the interfacial polarization effect [also named Maxwell–Wagner–Sillar (MWS) effect], which is ascribed to the accumulation of many charge carriers at the internal interfaces between MWNTs and PA11. According to the MWS effect, charges can be accumulated at the interface between two dielectric materials with different relaxation times by τ ($=\varepsilon/\sigma$, where ε is the dielectric constant and σ is the electrical conductivity) when current flows across the interface.[47] As MWNTs content increases, more charges will be accumulated at the interface resulting in higher dielectric constant but when MWNTs content reaches the percolation level, the accumulated charges will decrease in the form of current loss because of the formation of sophisticated electric conductive network. Besides the MWS effect, another

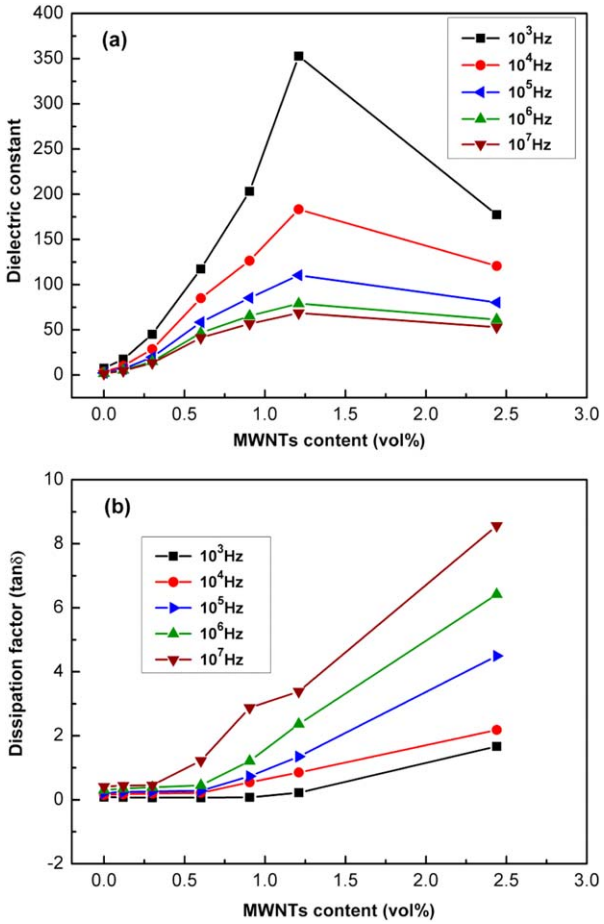

Figure 7. Dependence of (a) dielectric constant; (b) dielectric loss of pure PA11 and PA11/MWNTs composites on the MWNTs contents at the variation of frequency from 10^3 to 10^7 Hz. [Color figure can be viewed in the online issue, which is available at wileyonlinelibrary.com.]

mechanism named nanocapacitance-structure model can explain the increase of dielectric constant. Based on this model, the neighboring MWNTs isolated by matrix can be considered as nanoelectrodes and the thin layer of polymer between MWNTs acts as the nanodielectrics, forming abundant nanocapacitors in the composites. As the MWNTs content increases, the number of nanocapacitors increases, and the capacitance of a single nanocapacitor increases resulting from the decreases of the isolation distance between the MWNTs, both of which bring about high overall capacitance and thus high dielectric constant. Figure 7(b) exhibits the variation of dielectric dissipation factor (dielectric loss) as a function of MWNTs concentration at 10^3, 10^4, 10^5, 10^6, and 10^7 Hz. Dielectric loss refers to the dielectric materials generating heat in alternating electric field as a result of the electricity consumption. The lower is the dissipation factor of a dielectric material, the better performance of its charge storage applications. In general, for conductor/polymer composites, the dielectric loss is mainly regarded as the contribution of two distinct effects: direct current conductance and interfacial polarization, which have been reported in previous works.[48,49] The loss of direct current conductance dominates at low frequencies, while the loss of interfacial polarization dominates at high frequencies. It can be seen that the dielectric dissipation factor increases slightly with increasing MWNTs content, and then increases rapidly to about 1.6 when the MWNTs content reaches 2.44 vol % at 10^3 Hz, much higher than that of 0.05 and 0.2 for the pure PA11 and composites with 1.21 vol % MWNTs. As depicted in the electric conductivity section above, for the composites with 2.44 vol % MWNTs, the direct connection of MWNTs (MWNTs network) or the small distance between MWNTs will lead to a high direct current conductance, which contributes to high dielectric loss. Furthermore, a relatively weak frequency dependence of dielectric loss is obtained for the composites with low MWNTs content, while the dielectric loss is strongly dependent on the frequency for the composites with high MWNTs. It can be understood by the fact that interfacial polarization plays a more important role in dielectric properties than the nanocapacitors at high frequency, and the charge carriers and permanent dipoles are difficult to keep pace with the rapidly changing electric field when the frequency is sufficiently high.

CONCLUSION

PA11/MWNTs composites with excellent dielectric properties have been successfully prepared through melt blending method. SEM images of PA11/MWNTs composites reveal that MWNTs are dispersed uniformly in the composites. XRD, FTIR, and DSC results demonstrate that MWNTs can favor the formation of α crystal phase of PA11 when the composites are quenched from melt, while the pure PA11 represents the δ' phase. It is characterized that the electrical network of composites has formed with increasing MWNTs content determined by the direct current and alternating current conductivity results. The dielectric constant and dielectric loss of composites are strongly dependent on the frequency and MWNTs content. The dielectric constant of composite is as high as 350 at 10^3 Hz when the MWNTs content is 1.21 vol %, almost 50 times that of the pure PA11, accompanied by a relatively low dielectric loss of 0.2. These properties could facilitate the wide applications of composites as dielectric materials. It can be interpreted that the high dielectric constant and low dielectric loss derive from the formation of numerous nanocapacitors and the charge accumulation at interface between PA11 and MWNTs dispersed in the composites.

ACKNOWLEDGMENTS

This research was supported by the National Natural Science Foundation of China (Grant No. 51103087, 51421061). Authors wish to acknowledge Dr. Chaoliang Zhang (West China College of Stomatology, Sichuan University) for the SEM observation.

REFERENCES

1. Shen, Y.; Lin, Y.; Nan, C. W. *Adv. Funct. Mater.* **2007**, *17*, 2405.
2. Gallone, G.; Carpi, F.; De Rossi, D.; Levita, G.; Marchetti, A. *Mater. Sci. Eng. C* **2007**, *27*, 110.
3. Dang, Z.-M.; Xie, D.; Shi, C.-Y. *Appl. Phys. Lett.* **2007**, *91*, 222902.

4. Arbatti, M.; Shan, X.; Cheng, Z. Y. *Adv. Mater.* **2007**, *19*, 1369.
5. Barrau, S.; Demont, P.; Peigney, A.; Laurent, C.; Lacabanne, C. *Macromolecules* **2003**, *36*, 5187.
6. Kim, Y. J.; Shin, T. S.; Choi, H. D.; Kwon, J. H.; Chung, Y.-C.; Yoon, H. G. *Carbon* **2005**, *43*, 23.
7. Ahmad, K.; Pan, W.; Shi, S.-L. *Appl. Phys. Lett.* **2006**, *89*, 133122.
8. Yu, A.; Itkis, M. E.; Bekyarova, E.; Haddon, R. C. *Appl. Phys. Lett.* **2006**, *89*, 133102.
9. Islam, M.; Rojas, E.; Bergey, D.; Johnson, A.; Yodh, A. *Nano Lett.* **2003**, *3*, 269.
10. Dang, Z.-M.; Yao, S.-H.; Xu, H.-P. *Appl. Phys. Lett.* **2007**, *90*, 012907.
11. Zhang, S.; Zhang, N.; Huang, C.; Ren, K.; Zhang, Q. *Adv. Mater.* **2005**, *17*, 1897.
12. Li, Q.; Xue, Q.; Hao, L.; Gao, X.; Zheng, Q. *Compos. Sci. Technol.* **2008**, *68*, 2290.
13. Garnett, J. M. *Philos. Trans. R Soc. Lond. Ser A* **1906**, *205*, 237.
14. Tuncer, E.; Gubański, S. M.; Nettelblad, B. *J. Appl. Phys.* **2001**, *89*, 8092.
15. Jayasundere, N.; Smith, B. *J. Appl. Phys.* **1993**, *73*, 2462.
16. Zakri, T.; Laurent, J.-P.; Vauclin, M. *J. Phys. D Appl. Phys.* **1998**, *31*, 1589.
17. Nan, C.-W. *Prog. Mater. Sci.* **1993**, *37*, 1.
18. Dang, Z.-M.; Wang, L.; Wang, H.-Y.; Nan, C.-W.; Xie, D.; Yin, Y.; Tjong, S. *Appl. Phys. Lett.* **2005**, *86*, 172905.
19. Dang, Z.-M.; Wu, J.-B.; Fan, L.-Z.; Nan, C.-W. *Chem. Phys. Lett.* **2003**, *376*, 389.
20. Yang, Y.; Gupta, M. C.; Dudley, K. L.; Lawrence, R. W. *Nanotechnology* **2004**, *15*, 1545.
21. He, F.; Fan, J.; Lau, S. *Polym. Test.* **2008**, *27*, 964.
22. Yuan, J.-K.; Yao, S.-H.; Dang, Z.-M.; Sylvestre, A.; Genestoux, M.; Bai1, J. *J. Phys. Chem. C* **2011**, *115*, 5515.
23. Ning, N.; Bai, X.; Yang, D.; Zhang, L.; Lu, Y.; Nishi, T.; Tian, M. *RSC Adv.* **2014**, *4*, 4543.
24. Li, Q.; Xue, Q.; Zheng, Q.; Hao, L.; Gao, X. *Mater. Lett.* **2008**, *62*, 4229.
25. Yang, C.; Lin, Y.; Nan, C. *Carbon* **2009**, *47*, 1096.
26. Mei, B.; Scheinbeim, J.; Newman, B. *Ferroelectrics* **1995**, *171*, 177.
27. Mathur, S.; Scheinbeim, J.; Newman, B. *J. Appl. Phys.* **1984**, *56*, 2419.
28. Lee, J.; Takase, Y.; Newman, B.; Scheinbeim, J. *J. Polym. Sci. B Polym. Phys.* **1991**, *29*, 279.
29. Qingxin Zhang, Z. M.; Zhang, H.; Liu, S.; Cheng, S. Z. D. *Polymer* **2001**, *42*, 5543.
30. Nair, S. S.; Ramesh, C.; Tashiro, K. *Macromolecules* **2006**, *39*, 2841.
31. Panda, M.; Srinivas, V.; Thakur, A. *Appl. Phys. Lett.* **2008**, *93*, 242908.
32. Huang, X.; Jiang, P.; Xie, L. *Appl. Phys. Lett.* **2009**, *95*, 242901.
33. Yang, D. D.; Xu, H. P.; Wang, J. R.; Wu, Y. h. *J. Appl. Polym. Sci.* **2013**, *130*, 3746.
34. Liu, S.; Yu, Y.; Cui, Y.; Zhang, H.; Mo, Z. *J. Appl. Polym. Sci.* **1998**, *70*, 2371.
35. Wu, T. M.; Chen, E. C. *Polym. Eng. Sci.* **2006**, *46*, 1309.
36. Anand, K. A.; Agarwal, U.; Joseph, R. *Polymer* **2006**, *47*, 3976.
37. Li, J.; Fang, Z.; Tong, L.; Gu, A.; Liu, F. *J. Polym. Sci. B Polym. Phys.* **2006**, *44*, 1499.
38. Li, L.; Li, C. Y.; Ni, C.; Rong, L.; Hsiao, B. *Polymer* **2007**, *48*, 3452.
39. Yang, Z.; Huang, S.; Liu, T. *J. Appl. Polym. Sci.* **2011**, *122*, 551.
40. Takase, Y.; Lee, J.; Scheinbeim, J.; Newman, B. *Macromolecules* **1991**, *24*, 6644.
41. Sasaki, T. *J. Polym. Sci. B Polym. Lett.* **1965**, *3*, 557.
42. Jakeš, J.; Krimm, S. *Spectrochim. Acta A Mol. Spectrosc.* **1971**, *27*, 19.
43. Dang, Z. M.; Wang, L.; Yin, Y.; Zhang, Q.; Lei, Q. Q. *Adv. Mater.* **2007**, *19*, 852.
44. Barrau, S.; Demont, P.; Peigney, A.; Laurent, C.; Lacabanne, C. *Macromolecules* **2003**, *36*, 5187.
45. Zhu Jun, Z. X. *Chin. J. Chem. Phys.* **2005**, *18*, 631.
46. Balizer, E.; Fedderly, J.; Haught, D.; Dickens, B.; Dereggi, A. *J. Polym. Sci. B Polym. Phys.* **1994**, *32*, 365.
47. Tamura, R.; Lim, E.; Manaka, T.; Iwamoto, M. *J. Appl. Phys.* **2006**, *100*, 114515.
48. Li, Y.; Chen, C.; Li, J.-T.; Zhang, S.; Ni, Y.; Cai, S.; Huang, J. *Nanoscale Res. Lett.* **2010**, *5*, 1170.
49. Dang, Z.-M.; Wu, J.-P.; Xu, H.-P.; Yao, S.-H.; Jiang, M.-J.; Bai, J. *Appl. Phys. Lett.* **2007**, *91*, 072912.